Physics of Plasmas

Zeroth radial modes of azimuthal surface waves in dense plasma-loaded, coaxial helix traveling-wave-tube-like waveguides

Cite as: Phys. Plasmas **28**, 043106 (2021); https://doi.org/10.1063/5.0045139
Submitted: 25 January 2021 . Accepted: 06 April 2021 . Published Online: 30 April 2021

Igor O. Girka, Ivan V. Pavlenko, and Manfred Thumm

Physics of Plasmas ARTICLE scitation.org/journal/php

Zeroth radial modes of azimuthal surface waves in dense plasma-loaded, coaxial helix traveling-wave-tube-like waveguides

Cite as: Phys. Plasmas **28**, 043106 (2021); doi: 10.1063/5.0045139
Submitted: 25 January 2021 · Accepted: 6 April 2021 ·
Published Online: 30 April 2021

Igor O. Girka,[1,a)] Ivan V. Pavlenko,[1] and Manfred Thumm[2]

AFFILIATIONS

[1]V. N. Karazin Kharkiv National University, Svobody Sq., 4, 61022 Kharkiv, Ukraine
[2]Karlsruhe Institute of Technology, IHM and IHE, 76131 Karlsruhe, Germany

[a)]**Author to whom correspondence should be addressed:** igorgirka@karazin.ua

ABSTRACT

An analytical model of coaxial traveling-wave-tube-like waveguides with plasma filling has been justified and utilized to analyze the eigenmodes. Very often, introducing plasma into vacuum electronic devices leads to essential advantages as compared with evacuated tubes. The cylindrical structure under the present consideration consists of a central dielectric rod, placed inside a plasma coaxial layer with a metallic helix sheath on its outer interface, and a metal screen separated from the plasma by another dielectric layer. The dispersion properties of electromagnetic waves propagating across the external axial static magnetic field in such traveling-wave-tube-like waveguides are studied and summarized. The presence of a dense plasma coaxial layer makes the media nontransparent for waves in the electron cyclotron frequency range. However, surface type electromagnetic waves can propagate in this case. These waves are called azimuthal surface waves (ASWs). The helix sheath causes coupling of ordinarily and extraordinarily polarized ASWs. The zeroth radial ASW modes have been found to be most dangerous for parasitic wave excitation in dense plasma-loaded, coaxial traveling-wave-tube-like waveguides.

I. INTRODUCTION

Traveling wave tubes (TWTs) are widely applied in telecommunication and therefore intensively studied in the scientific literature. A comprehensive overview of their development since 1942 till nowadays has been presented in Ref. 1. Their potential impact on commercial and industrial applications explains the continuous interest in further improving their technical characteristics.

The dispersion relation for the relativistic TWT was derived in the framework of the linear field theory and analyzed in Ref. 2. The TWT was assumed to be filled by a cold and uniform plasma. The slow-wave structure was considered to be sinusoidally corrugated and driven by a finite thick annular intense relativistic electron beam with the entire system immersed in a strong axial magnetic field. A similar TWT structure with an elliptical cross section and a degenerate plasma column protected by an elliptical annular dielectric layer was theoretically investigated in Ref. 3.

Forward- and backward-wave interaction was analyzed in Ref. 4 following the Eulerian hydrodynamic approach in a plasma-filled helix TWT, taking into account the following three features. First, the velocity of plasma electrons was considered to be thermal. Second, collisions between plasma electrons were taken into account. Third, the effect of the finite radius of the electron beam and its proximity to a metal wall was studied.

Variable-width technology was applied in Ref. 5 to folded waveguide TWTs to suppress the lower band edge oscillation and to expand the operating frequency bandwidth. An output power level of over 350 W in the W-band frequency range of 85–90 GHz (5 GHz) was obtained with a maximum power of ∼648 W and an electron efficiency of ∼12.1% at 88 GHz with a beam current of 260 mA and a beam voltage of 20.5 kV.

A 340 GHz integrated dual-beam TWT based on a staggered dual-vane slow-wave structure was investigated in Ref. 6. A uniform magnetic field of 0.52 T was utilized to focus the two electron beams, and a beam transmission efficiency of 97.1% was achieved over the TWT length of 50 mm.

A 1D frequency-domain nonlinear model was studied in Ref. 7 for illustrating the beam-wave interaction in sinusoidal-waveguide (SWG) TWTs. The model took into account space-charge fields and Ohmic losses to be closer to practical situations. The sheath beam was split into a set of rectangular electron plates in the axial direction, and

the space-charge field was calculated in the framework of the theory of Green's function. The model was successfully applied to the design of a 0.22 THz SWG TWT.

The interaction of electromagnetic waves and electron beams in a 4-m-long TWT was investigated in Ref. 8. The device was specifically designed to provide low-noise beam-plasma experiments. The nonlinear phenomena arising from the beam–wave interaction, such as the modulation of the electron beam, the wave growth, and the saturation process were analyzed also.

The dielectric-plasma-vacuum-metal structure considered in the present paper is almost the same as that studied in Ref. 9. However, the following essential features are different. First, in Ref. 9 the azimuthal wavenumber m was equal to zero and wave propagation in the axial direction was studied. On the contrary, flute electromagnetic waves with $k_z = 0$ and $m \neq 0$ are considered in the present paper. Second, in Ref. 9 the plasma was assumed to be degenerate, whereas a magnetoactive gas plasma is considered here.

Azimuthal surface waves (ASWs) are known to be electromagnetic eigenwaves of cylindrical plasma-filled waveguides.[10] Therefore, they are described in cylindrical coordinates, having the axis along both the waveguide axis and the external magnetic field direction. They are intensively studied due to their possible applications in plasma electronics, plasma-antenna systems, plasma production, and nano-technologies.[11–18] Plasma electronics devices are well known to have several advantages compared with vacuum devices, since they are characterized by a wider spectrum of eigenfrequencies. Therefore, they provide the possibility to control the frequency spectrum in a wide frequency range, to generate and/or enhance radiation in superhigh frequency ranges and the possibility to enhance electromagnetic radiation power generated by these devices due to the ability to increase the electric current, which flows in the plasmas.

The dependencies of ASW electromagnetic fields on the coordinates and time are as follows: $f(r)\exp[i(m\varphi - \omega t)]$. Here, r is the radial coordinate, m the azimuthal wavenumber (m is an integer), φ the azimuth angle, ω the wave angular frequency, and t the time. ASWs of ordinary polarization (OASWs) with the field components H_r, H_φ, E_z and those with extraordinary polarization (XASWs) with the components E_r, E_φ, H_z are known to propagate independently in the external axial static magnetic field. The presence of a nonzero axial wavenumber k_z and/or an azimuthal component of the external static magnetic field would cause coupling of the ordinary and extraordinary ASWs.[19–21] In these cases, ordinary and extraordinary ASWs cannot be considered separately.

In the present paper, dispersion properties of coupled ASWs are studied in the case when the coupling is caused by the presence of the metallic helix, the slow-wave structure in TWTs. The dispersion relation of ASWs is derived for the structure, which consists of a cylindrical dielectric rod (for helix support) placed inside the magnetoactive plasma coaxial layer with a cylindrical helix sheath (similar to a tape helix) on its outer interface, and one dielectric coaxial layer more, which separates the structure from the outer cylindrical metal wall (Fig. 1). The latter dielectric layer is usually vacuum and is used for transmission of an annular electron beam in the axial direction. The dispersion relation has the form of the determinant of an 8×8 matrix. The dependencies of the eigenfrequency on the geometrical dimensions, plasma particle density, axial static magnetic field, magnitude and sign of azimuthal wavenumber, helix pitch angle, and dielectric constants are studied numerically.

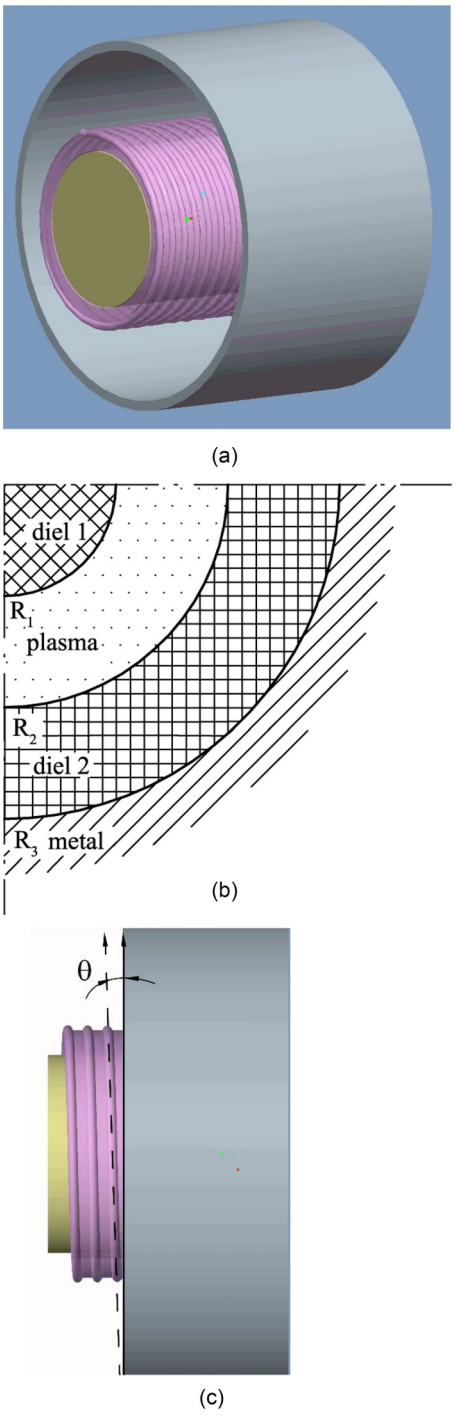

FIG. 1. (a) Schematic of the problem. General view. (b) Cross section of the waveguide. The space $r \leq R_1$ is occupied by the dielectric rod. Plasma is placed in the layer $R_1 \leq r \leq R_2$. The metallic helix sheath (similar to a tape helix) is placed at the interface $r = R_2$. The other dielectric layer, $R_2 \leq r \leq R_3$, separates the plasma from the metal wall. (c) To the definition of the helix pitch angle.

The paper is arranged as follows. After the present introduction (Sec. I), the model of the plasma waveguide to be studied is described in Sec. II. The spatial distribution of the ASW field is presented along with the boundary conditions. The dispersion relation is also derived in the form of the determinant of the 8×8 matrix. The elements of the matrix are listed in the Appendix. The numerical analysis of the dispersion relation is carried out in Sec. III. Finally, the conclusions are summarized in Sec. IV.

II. PLASMA WAVEGUIDE MODEL AND DERIVATION OF DISPERSION RELATION

As described in Sec. I, a three-component cylindrical waveguide structure is considered (see Fig. 1) in the present paper. It is assumed to be infinite and uniform in the axial direction. The external static magnetic field only has an axial component ($\vec{B}_0 || \vec{z}$).

A cylindrical dielectric rod with dielectric constant ε_{d1} and radius R_1 is placed in the center of the metal waveguide with radius R_3. The radial distribution of the fields of ASWs within the rod can be found from Maxwell's equations. Taking into account the boundary condition at the axis of the system, one can express the amplitude of the axial component of the ASW magnetic field, $B_z(\vec{r}) = B_z(r) \exp[i(m\varphi - \omega t)]$ as

$$B_z(r) = A_1 J_m(k_{d1} r), \quad r < R_1. \tag{1}$$

In Eq. (1), A_1 is a constant of integration, $J_m(\xi)$ is the Bessel function of the first kind of the order m,[22] $k_{d1} = k\sqrt{\varepsilon_{d1}}$, $k = \omega/c$, and c is the speed of light in vacuum.

The amplitudes of the radial and azimuthal components of ASW electric fields can be derived in terms of $B_z(r)$

$$E_r(r) = -\frac{km}{k_{d1}^2 r} B_z, \quad E_\varphi(r) = -\frac{ik}{k_{d1}^2} \frac{dB_z}{dr}. \tag{2}$$

The radial distribution of the axial component of the ASW electric field can also be found as a solution of the Bessel equation

$$E_z(r) = A_2 J_m(k_{d1} r), \quad r < R_1. \tag{3}$$

The amplitudes of the radial and azimuthal components of ASW magnetic fields can be written in terms of $E_z(r)$ within the whole waveguide, $0 \le r \le R_3$, as follows:

$$B_r(r) = \frac{m}{kr} E_z, \quad B_\varphi(r) = \frac{i}{k} \frac{dE_z}{dr}. \tag{4}$$

The inner rod in covered by the coaxial plasma layer with internal radius R_1 and external radius R_2. The tangential components of ASW electric and magnetic fields should be continuous at the boundary $r = R_1$.

The plasma is assumed to be cold and collisionless. In such a plasma, the displacement vector $\vec{D}$ is linked with the electric field $\vec{E}$ via the permittivity tensor[23]

$$\hat{\varepsilon} = \begin{pmatrix} \varepsilon_1 & i\varepsilon_2 & o \\ -i\varepsilon_2 & \varepsilon_1 & 0 \\ 0 & 0 & \varepsilon_3 \end{pmatrix}. \tag{5}$$

Its components read as

$$\varepsilon_1 = 1 - \sum_\alpha \frac{\Omega_\alpha^2}{\omega^2 - \omega_\alpha^2}, \quad \varepsilon_2 = -\sum_\alpha \frac{\Omega_\alpha^2 \omega_\alpha}{\omega(\omega^2 - \omega_\alpha^2)}, \quad \varepsilon_3 = 1 - \sum_\alpha \frac{\Omega_\alpha^2}{\omega^2}. \tag{6}$$

In Eq. (6), Ω_α is plasma frequency of the particle of species α ($\alpha = i$ for ions and $\alpha = e$ for electrons), and ω_α is corresponding cyclotron frequency.

In the following, the plasma is assumed to be uniform and sufficiently dense, and the external static magnetic field is assumed to be sufficiently weak, $\Omega_e > |\omega_e|$. The dispersion properties of XASWs in the opposite case of strongly magnetized plasma were studied in Ref. 24. In this case, surface type oscillations of ion species were demonstrated to be possible. Excitation of XASWs by annular ion beams was shown in Ref. 25 to take place under extremely strong external static axial magnetic field.

The amplitude of the ASW axial magnetic field can be written in terms of the modified Bessel functions of the first, $I_m(\xi)$, and second, $K_m(\xi)$, kinds[22]

$$B_z(r) = B_1 I_m(k_\perp r) + B_2 K_m(k_\perp r), \; R_1 < r < R_2. \tag{7}$$

Here, B_1 and B_2 are the constants of integration. The penetration depth $k_\perp^{-1}$ of the XASW into the plasma is defined as follows: $k_\perp^2 = k^2 \varepsilon_1 (\mu^2 - 1)$, with $\mu = \varepsilon_2/\varepsilon_1$. The electromagnetic wave field is of surface nature just inside the plasma coaxial layer. Outside of the plasma, the considered waves are of bulk nature. This is true within specific frequency ranges only. These ranges were defined in Ref. 26 from the inequality $k_\perp^2 > 0$

$$\omega_{LH} < \omega < |\omega_e|, \quad |\omega_e| < \omega < \omega_1, \tag{8}$$

$$\omega_{UH} < \omega < \omega_2, \tag{9}$$

where $\omega_{1,2} = \mp|\omega_e|/2 + \sqrt{\Omega_e^2 + \omega_e^2/4}$ are the cutoff frequencies for bulk modes, and ω_{LH} and ω_{UH} are the lower and upper hybrid frequencies, respectively. These ranges (8) and (9) were referred to as low-frequency (LF) and high-frequency (HF) region, respectively. At first view, these ranges should be out of scope of practical application since the plasma is nontransparent for electromagnetic waves in this case. On the other hand, electromagnetic wave excitation in these ranges can be more efficient since one has to spend less energy to build up the structure of surface type waves than that for bulk waves. XASWs of the frequency range (9) propagate with higher frequencies, which can be of interest for practical applications. However, excitation of XASWs by gyrating electron beams above the upper hybrid frequency was found to be less efficient than in the range of electron cyclotron frequency.[27,28] That is why the LF range is considered in the present paper.

The amplitudes of XASW electric fields can be written in terms of $B_z(r)$

$$E_r(r) = \frac{k}{k_\perp^2}\left(\mu \frac{dB_z}{dr} + \frac{m}{r} B_z\right), \quad E_\varphi(r) = \frac{ik}{k_\perp^2}\left(\frac{dB_z}{dr} + \frac{\mu m}{r} B_z\right). \tag{10}$$

Within the plasma layer, OASWs are also of surface nature. The amplitude of the electric field of OASWs reads as follows:

$$E_z(r) = B_3 I_m(k_o r) + B_4 K_m(k_o r), \quad R_1 < r < R_2. \tag{11}$$

The penetration depth of OASWs into the plasma k_o^{-1} is defined as follows:

$$k_o = k\sqrt{-\varepsilon_3}.$$

The outer interface of the plasma layer at $r = R_2$ is defined by the metallic helix sheath (tape helix). This sheath is assumed to be a surface with zero thickness and anisotropic electrical conductivity. The sheath is characterized by the helix pitch angle $\theta = arctan[d/(2\pi R_2)]$ with d being the axial progression length of the tape helix, which is the angle between the tangent to the tape and the azimuthal direction [Fig. 1(c)]. The electrical conductivity is assumed to be infinite along the tape and zero in the direction perpendicular to the tape. That is why at this interface, the tangential components of the ASW electric fields E_φ and E_z should be continuous, the longitudinal ASW electric field should vanish, which means $\sin\theta\, E_z + \cos\theta\, E_\varphi = 0$, and the longitudinal ASW magnetic field should be continuous as well. These two last boundary conditions cause the coupling of XASWs and OASWs.

The coaxial plasma layer with the outer helix sheath is separated from the cylindrical metal wall by a coaxial dielectric layer with the dielectric constant ε_{d2}. The radial distribution of the ASW fields within this layer can be written in terms of Bessel functions of the first and second, $N_m(\xi)$, kinds:[22]

$$B_z(r) = C_1\left[J_m(k_{d2}r)N'_m(k_{d2}R_3) - N_m(k_{d2}r)J'_m(k_{d2}R_3)\right], \quad R_2 < r < R_3, \tag{12}$$

$$E_z(r) = C_2[J_m(k_{d2}r)N_m(k_{d2}R_3) - N_m(k_{d2}r)J_m(k_{d2}R_3)], \quad R_2 < r < R_3. \tag{13}$$

In Eqs. (12) and (13), C_1 and C_2 are constants of integration, and $k_{d2} = k\sqrt{\varepsilon_{d2}}$. A prime denotes the derivative of the function with respect to the argument.

The amplitudes of the radial and azimuthal components of the ASW electric fields can be presented in the form of Eq. (2) with the following replacement: $\varepsilon_{d1} \to \varepsilon_{d2}$. The amplitude of the radial and azimuthal components of the ASW magnetic fields can be written in terms of $E_z(r)$ in the form of Eq. (4). The expressions (12) and (13) already satisfy the boundary conditions at the metal wall, which mean that the ASW tangential electric fields $E_\varphi(r)$ and $E_z(r)$ vanish at the interface $r = R_3$.

The boundary conditions mentioned above make it possible to derive the dispersion relation for ASWs in the considered waveguide in the form of the determinant of an 8×8 matrix

$$det a_{ij} = 0. \tag{14}$$

The elements of the matrix a_{ij} are summarized in the Appendix.

Here, one should underline that the dispersion relation of symmetric ($m = 0$ and axial wavenumber $k_z \neq 0$) electromagnetic waves in the same waveguide structure as in the present paper but with a degenerate plasma was investigated in Ref. 9. There, the dispersion relation was derived in the form of the determinant of a 10×10 matrix.

III. NUMERICAL ANALYSIS OF THE DISPERSION RELATION

Figures 2–6 show the results of the numerical analysis of the dispersion relation (14). There, the ASW eigenfrequency normalized by the electron cyclotron frequency, $\omega/|\omega_e|$, is given as ordinate. Figure 7 is the only exception, where the influence of the external static magnetic field is studied. That is why the choice of $|\omega_e|$ for frequency normalization is inappropriate there. Therefore, in Fig. 7 the ASW eigenfrequency is normalized by the electron plasma frequency and ω/Ω_e is the ordinate.

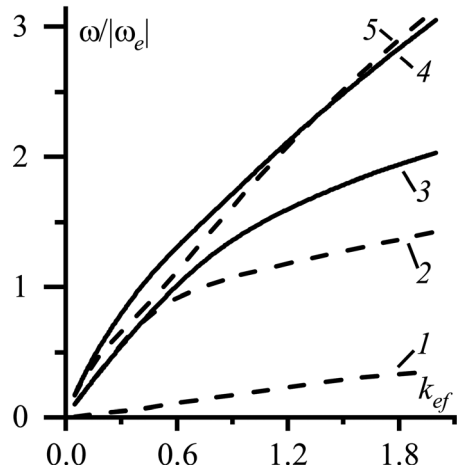

FIG. 2. Normalized ASW eigenfrequency vs k_{ef} for opposite directions of the wave propagation. $\theta = \pi/3$, $Z \equiv \Omega_e/|\omega_e| = 5$, $\varepsilon_{d1} = 6.4$, $\varepsilon_{d2} = 1$, $R_2/R_1 = 2.0$, and $R_3/R_1 = 3.0$, $m = -1$ (two solid curves), $m = +1$ (three dashed curves): "1"—lower branch of the dispersion curve for ASW with $m = +1$; "2"—middle branch of the dispersion curve for ASW with $m = +1$; "3"—middle branch of the dispersion curve for ASW with $m = -1$; "4"—upper branch of the dispersion curve for ASW with $m = -1$; "5"—upper branch of the dispersion curve for ASW with $m = +1$.

The effective azimuthal wavenumber, $k_{ef} = |m|\delta/R_1$, is chosen as abscissa. Here, $\delta = c/\Omega_e$ is the skin-depth. This choice of the abscissa is explained by the following. It is usual to present dispersion curves with the variables "wavenumber-frequency." The ratio $|m|/R_1$ plays

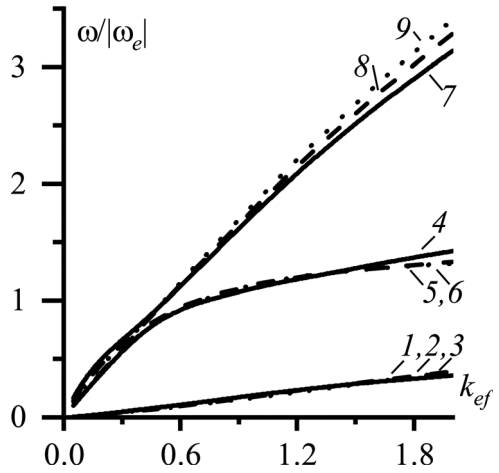

FIG. 3. Normalized ASW eigenfrequency vs k_{ef} for positive magnitudes of azimuthal wavenumber. $m = +1$ (solid curves), $m = +2$ (dashed curves), $m = +3$ (dotted curves), $\theta = \pi/3$, $Z = 5$, $\varepsilon_{d1} = 6.4$, $\varepsilon_{d2} = 1$, $R_2/R_1 = 2.0$, and $R_3/R_1 = 3.0$: "1,2,3"—lower branches of the dispersion curves; "4"—middle branch of the dispersion curve for ASW with $m = +1$; "5,6"—middle branches of the dispersion curves for ASW with $m = +2, 3$; "7"—upper branch of the dispersion curve for ASW with $m = +1$; "8"—upper branch of the dispersion curve for ASW with $m = +2$; "9"—upper branch of the dispersion curve for ASW with $m = +3$.

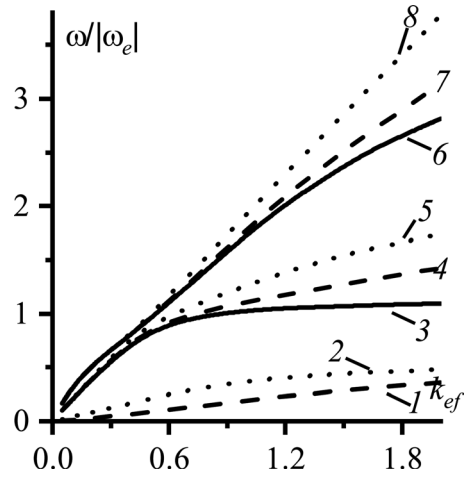

FIG. 4. Normalized ASW eigenfrequency vs k_{ef} for different helix pitch angles. $\theta = \pi/2$ (two solid curves), $\theta = \pi/3$ (three dashed curves), $\theta = \pi/6$ (three dotted curves), $m = +1$, $Z = 5$, $\varepsilon_{d1} = 6.4$, $\varepsilon_{d2} = 1$, $R_2/R_1 = 2.0$, $R_3/R_1 = 3.0$: "1"—lower branch of the dispersion curve for the helix pitch angle $\theta = \pi/3$; "2"—lower branch of the dispersion curve for the helix pitch angle $\theta = \pi/6$; "3"—middle branch of the dispersion curve for the helix pitch angle $\theta = \pi/2$; "4"—middle branch of the dispersion curve for the helix pitch angle $\theta = \pi/3$; "5"—middle branch of the dispersion curve for the helix pitch angle $\theta = \pi/6$; "6"—upper branch of the dispersion curve for the helix pitch angle $\theta = \pi/2$; "7"—upper branch of the dispersion curve for the helix pitch angle $\theta = \pi/3$; "8"— upper branch of the dispersion curve for the helix pitch angle $\theta = \pi/6$.

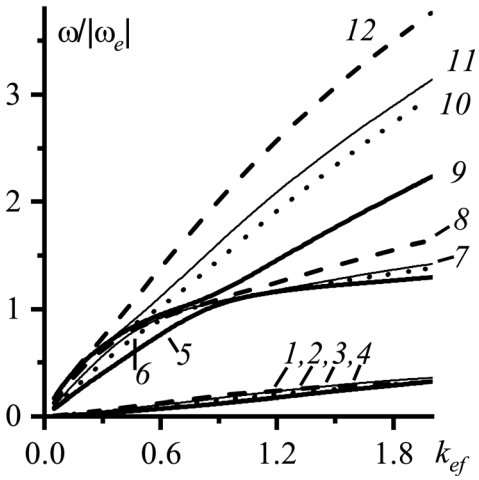

FIG. 5. Normalized ASW eigenfrequency vs k_{ef} for different dimensions of the waveguide components. $R_2/R_1 = 2.0$, $R_3/R_1 = 3.0$ (thin solid curves), $R_2/R_1 = 1.6$, $R_3/R_1 = 2.4$ (bold solid curves), $R_2/R_1 = 2.0$, $R_3/R_1 = 4.0$ (dashed curves), $R_2/R_1 = 3.0$, $R_3/R_1 = 4.0$ (dotted curves), $m = +1$, $\theta = \pi/3$, $Z = 5$, $\varepsilon_{d1} = 6.4$, and $\varepsilon_{d2} = 1$: "1,2,3,4"—lower branches of the dispersion curves for all the four configurations; "5"—middle branch of the dispersion curve for the configuration with increased dielectric rod radius; "6"—middle branch of the dispersion curve for the configuration with increased plasma layer width; "7"—middle branch of the dispersion curve for the initial configuration ($R_2/R_1 = 2.0$, $R_3/R_1 = 3.0$); "8"—middle branch of the dispersion curve for the configuration with increased external dielectric layer width; "9"—upper branch of the dispersion curve for the configuration with increased dielectric rod radius; "10"—upper branch of the dispersion curve for the configuration with increased plasma layer width; "11"—upper branch of the dispersion curve for the initial configuration; "12"—upper branch of the dispersion curve for the configuration with increased external dielectric layer width.

the role of the characteristic azimuthal wavenumber in the present paper. After normalization by the skin-depth, the ratio becomes the effective wavenumber. Therefore, Figs. 2–7 show the dependencies of ASW eigenfrequencies on either the plasma particle density n_e (since $k_{ef} \propto n_e^{-1/2}$) or the dielectric rod radius R_1.

The higher the radial wavenumber (the number of nodes of the radial field distribution within the dielectrics except of those at the axis and at the metal wall) is, the less efficient is the excitation of this wave (see, e.g., Ref. 29). That is why the zeroth radial modes are considered in the present paper. To be sure that the calculated frequency relates to just the zeroth radial mode one has to check whether the frequency shift, $[k_{d1}R_1 + k_{d2}(R_3 - R_2)]$, is smaller or of the order of π.

To demonstrate the difference between the dispersion properties of ASWs propagating in opposite directions, the dependencies of ASW eigenfrequencies on the effective wavenumber are presented in Fig. 2 for the azimuthal wavenumbers $m = \pm 1$. The dielectric constant of the inner rod is chosen as that of mica, $\varepsilon_{d1} = 6.4$, and the external coaxial dielectric layer is chosen as vacuum with $\varepsilon_{d2} = 1$, since its purpose in a TWT is to carry the annular electron beam. The following other parameters of the waveguide structure are chosen for the calculations: $m = -1$ (solid curves), $m = +1$ (dashed curves), $\theta = \pi/3$, $Z \equiv \Omega_e/|\omega_e| = 5$, $R_2/R_1 = 2.0$, $R_3/R_1 = 3.0$. The shape of the four upper curves in Fig. 2 is in qualitative agreement with those obtained in Refs. 10 and 26 wherein the space $r < R_1$ was filled by the plasma. The similarity is especially pronounced for small magnitudes of k_{ef}, which corresponds to the case of small ASW penetration depth into the plasma. In the latter case, $k_{ef} < 1$, the surface wave dispersion properties are insensitive to the permittivity of the internal media. One can see in Fig. 2 that the upper branches vary weakly with changing the sign of m. The frequencies of the middle branches of ASWs with $m > 0$ are significantly smaller than those of ASWs with $m < 0$. For example, for $|m| = 1$ and $k_{ef} = 2$, the difference is about 35%. The main qualitative difference between the dispersion properties of ASWs with opposite signs of azimuthal wavenumbers is that the dispersion relation for ASWs with positive m have three roots rather than two as for the case of $m < 0$. However, these additional frequencies ($\omega < 0.4 \mid \omega_e|$ in Fig. 2) of ASWs with positive m are much lower than those in the middle and upper branches, which make them less important for excitation in TWTs.

To study the influence of the absolute value of the azimuthal wavenumber on the dispersion properties of ASWs, the dependence of ASW eigenfrequencies on k_{ef} is plotted in Fig. 3 for the azimuthal wavenumbers $m = +1, +2, +3$. The other plasma waveguide parameters are the same as in Fig. 2. The difference between the three frequencies which correspond to the same magnitude of azimuthal wavenumber successively increases with increasing k_{ef} for smaller magnitudes of the plasma particle density, $k_{ef} > 1$. The difference between the ASW frequencies of the lower branches is almost invisible in Fig. 3.

The lower frequency branch of the ASW with $m = 2$ is larger by 10% than that for the ASW with $m = 1$ for $k_{ef} = 2.0$, and larger by 1% than that for $m = 3$. The middle frequency branch monotonously decreases with increasing $|m|$. The middle frequency branch of the ASW with $m = 1$ is larger than that for the ASW with $m = 2$ by 7% for

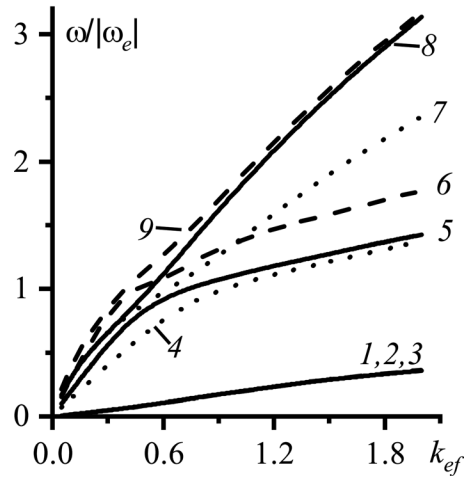

FIG. 6. Normalized ASW eigenfrequency vs k_{ef} for different dielectric constants of the internal dielectric rod. $\varepsilon_{d1} = 6.4$, $\varepsilon_{d2} = 1$ (solid curves), $\varepsilon_{d1} = 4.0$, $\varepsilon_{d2} = 1$ (dashed curves), $\varepsilon_{d1} = 6.4$, $\varepsilon_{d2} = 2$ (dotted curves), $m = +1$, $Z = 5$, $\theta = \pi/3$, $R_2/R_1 = 2.0$, and $R_3/R_1 = 3.0$: "1,2,3"—lower branches of the dispersion curves for all the three cases; "4"—middle branch of the dispersion curve in the case of larger dielectric constant of the external dielectric layer; "5"—middle branch of the dispersion curve in the initial case ($\varepsilon_{d1} = 6.4$, $\varepsilon_{d2} = 1$); "6"—middle branch of the dispersion curve in the case of smaller dielectric constant of the dielectric rod; "7"—upper branch of the dispersion curve in the case of larger dielectric constant of the external dielectric layer; "8"—upper branch of the dispersion curve in the initial case; "9"—upper branch of the dispersion curve in the case of smaller dielectric constant of the dielectric rod.

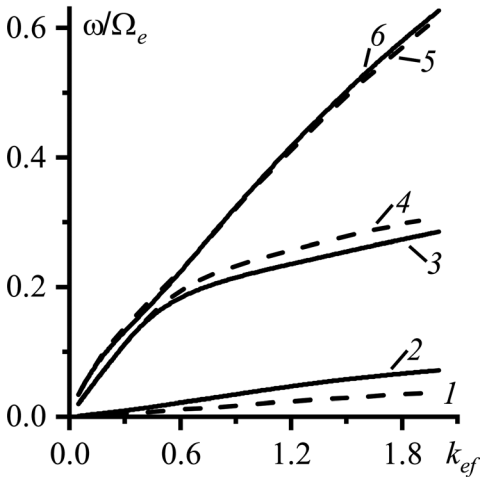

FIG. 7. Normalized ASW eigenfrequency vs k_{ef} for different magnitudes of the external static axial magnetic field. $Z = 5$ (solid curves), $Z = 10$ (dashed curves), $m = +1$, $\theta = \pi/3$, $\varepsilon_{d1} = 6.4$, $\varepsilon_{d2} = 1$, $R_2/R_1 = 2.0$, and $R_3/R_1 = 3.0$: "1"—lower branch of the dispersion curve in the case of smaller external static axial magnetic field B_0; "2"—lower branch of the dispersion curve in the case of larger B_0; "3"—middle branch of the dispersion curve in the case of larger B_0; "4"—middle branch of the dispersion curve in the case of smaller B_0; "5"—upper branch of the dispersion curve in the case of smaller B_0; "6"—upper branch of the dispersion curve in the case of larger B_0.

$k_{ef} = 2.0$, and larger than that for $m = 3$ by 8%. The upper frequency branch monotonously increases with increasing $|m|$. The upper frequency branch of the ASW with $m = 1$ is smaller than that for the ASW with $m = 2$ by 5% for $k_{ef} = 2.0$, and smaller than that for $m = 3$ by 9%.

The influence of the helix pitch angle θ on the ASW eigenfrequency is plotted in Fig. 4. In the case $\theta = \pi/2$ (see solid curves), the infinite electrical conductivity of the metal helix sheath in the axial direction suppresses the axial electric wave field, $E_z = 0$. In this case, ASWs propagate in the form of XASWs, and the dispersion relation has two roots. The dependence of the ASW eigenfrequency on k_{ef} for the helix pitch angle $\theta = \pi/3$ is presented in Fig. 4 by the dashed curves, and for $\theta = \pi/6$ by the dotted curves. One can see the gradual increase in the ASW frequency with decreasing pitch angle of the helix sheath. In the case $\theta = 0$, the azimuthal component of the wave electric field vanishes, $E_\varphi = 0$. Since the zeroth radial modes of OASWs do not propagate in the considered frequency ranges (8), (9), the dispersion relation (14) has no roots in this case.

The influence of the geometrical dimensions of the waveguide components on the ASW eigenfrequency is studied in Fig. 5. The thin solid curves are presented for the comparison of various different geometries for the case of equal widths of all the components of the waveguide structure under study: internal dielectric rod, plasma coaxial layer, and external dielectric layer ($R_2/R_1 = 2.0$, $R_3/R_1 = 3.0$). An increase in the dielectric rod radius R_1 by the factor of 1.25, while keeping the same ratio of the two other radii, R_3/R_2, is shown by the bold solid curves in Fig. 5 to cause a decrease in the ASW eigenfrequencies. Increasing radius of the metal wall and the resulting increase in the width of the external dielectric layer, while keeping the same ratio of the two other radii, $R_2/R_1 = 2.0$, results in increasing ASW frequencies (see dashed curves in Fig. 5). An increase in the width of the plasma layer, while keeping the same ratio of the external dielectric width to the radius of the dielectric rod, $(R_3 - R_2)/R_1$, causes decreasing ASW frequencies. All the changes in the geometrical dimensions mentioned above only have a weak influence on the lower branch of ASW frequencies. These curves ($\omega < 0.357|\omega_e|$) are almost indistinguishable in Fig. 5. The difference between the ASW frequencies in this branch is smaller than 12% for $k_{ef} = 2$.

A decrease in the magnitude of the permittivity of the dielectric rod from $\varepsilon_{d1} = 6.4$ ($\varepsilon_{d2} = 1$, solid curves) to $\varepsilon_{d1} = 4.0$ ($\varepsilon_{d2} = 1$, dashed curves) is shown in Fig. 6 to result in increasing ASW eigenfrequencies of the middle branch with almost no change in those of the upper and lower branches. One can see in Fig. 6 also, that increasing magnitude of the dielectric constant of the outer dielectric layer from $\varepsilon_{d2} = 1.0$ ($\varepsilon_{d1} = 6.4$, solid curves) to $\varepsilon_{d2} = 2.0$ ($\varepsilon_{d1} = 6.4$, dotted curves) would cause decreasing ASW eigenfrequencies of the upper branch with almost no change in those of the middle and lower branches. It was noted in Refs. 10 and 26 that an increase in the relative width of the external dielectric layer and a decrease in its dielectric constant lead to increasing XASW eigenfrequency. This is in qualitative agreement with the results presented in Figs. 5 and 6.

Figure 7 shows that a decrease in the external static axial magnetic field by a factor of two (which is equivalent to the enhancement of $Z \equiv \Omega_e/|\omega_e|$ from $Z = 5$ to $Z = 10$) causes a weak decrease in the ASW frequencies in the upper and lower branches and an increase in those in the middle branch. For example, for $k_{ef} = 2.0$ the ASW frequency in the upper branch decreases by about 2.8% and increases in the middle branch by about 7.8%.

In the following, the parameters of a practical laboratory device are estimated for which the results obtained in the present paper can be applied. If the external static axial magnetic field is $B_0 = 1.5$ kG, which is a typical magnitude for small-size TWTs, the angular electron cyclotron frequency is $|\omega_e| = 2.64 \times 10^{10}$ rad/s. The highest frequency $\omega = 3.039|\omega_e|$ is obtained in calculations for $k_{ef} = 1.6$, as shown in Fig. 4. Since $Z \equiv \Omega_e/|\omega_e| = 5$, the electron plasma frequency is $\Omega_e = 1.3 \times 10^{11}$ rad/s, which corresponds to the plasma particle density $n_e = 5.4 \times 10^{12}$ cm^{-3}. Applying this magnitude of k_{ef} and the azimuthal wavenumber $m = 1$ leads to the radius of internal dielectric rod $R_1 = 0.14$ cm, the external radius of the plasma coaxial layer $R_2 = 0.28$ cm, and that of the metal wall $R_3 = 0.42$ cm. All these parameters look like achievable in a University Laboratory. The ASW frequency is expected to belong to the gigahertz range, $\nu = 12.6$ GHz.

The analysis of the dispersion properties cannot be considered as completed without any comments on the wave field distribution. The radial distributions of ASW electric fields E_φ and E_z are plotted in Fig. 8 for the following parameters of the waveguide: $Z = 5$, $m = +2$, $\theta = \pi/3$, $\varepsilon_{d1} = 6.4$, $\varepsilon_{d2} = 1$, $R_2/R_1 = 2.0$, $R_3/R_1 = 3.0$, and $k_{ef} = 1.0$. The latter correspond to the data presented in Fig. 3 by dashed curves. All the pairs of curves are normalized in such a way that the maximum magnitude of the wave field amplitude E_φ within the waveguide is equal to one. The wave field amplitudes are given in arbitrary units.

In the considered frequency range, the zeroth radial modes of OASWs are not eigenwaves of the studied waveguide structure in the absence of the coaxial helix sheath. That is why they are driven oscillations in the present problem. This circumstance explains the fact that the normalized magnitude of E_z is smaller than one within the whole waveguide. The helix sheath provides the maximum magnitude of the field E_z just at $r = R_2$. These maximum magnitudes Max$\{E_z\}$ are equal to 0.594 for $\omega = 0.18|\omega_e|$ (solid curve), Max$\{E_z\} = 0.032$ for $\omega = 1.142|\omega_e|$ (dashed curve), and Max$\{E_z\} = 0.577$ for $\omega = 1.824|\omega_e|$ (dotted curve). The first and third curves (solid and dotted ones) are almost indistinguishable in Fig. 8.

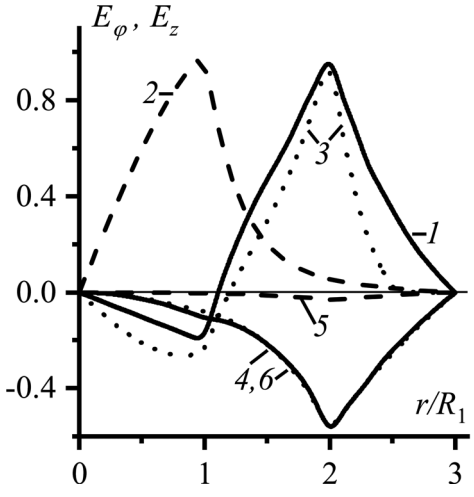

FIG. 8. Radial distribution of ASW electric fields E_φ and E_z (in arbitrary units). $\omega = 0.18|\omega_e|$ (solid curves), $\omega = 1.142|\omega_e|$ (dashed curves), and $\omega = 1.824|\omega_e|$ (dotted curves). The curves are normalized such that the maximum magnitude of E_φ within the waveguide is equal to one. $Z = 5$, $m = +2$, $\theta = \pi/3$, $\varepsilon_{d1} = 6.4$, $\varepsilon_{d2} = 1$, $R_2/R_1 = 2.0$, $R_3/R_1 = 3.0$, and $k_{ef} = 1.0$: "1"—$E_\varphi(r)$ for the lower branch of the ASW dispersion curve; "2"—$E_\varphi(r)$ for the middle branch of the dispersion curve; "3"—$E_\varphi(r)$ for the upper branch of the dispersion curve; "4,6"—$E_z(r)$ for the lower and upper branches of the dispersion curve; "1"—$E_z(r)$ for the middle branch of the dispersion curve.

The azimuthal electric fields of the modes that propagate with the lowest frequency $\omega = 0.18|\omega_e|$ and the highest one $\omega = 1.824|\omega_e|$ reach their maxima at the interface $r = R_2$. They both change their signs within the plasma layer. These changes of signs should not be considered as indicator of a higher radial mode, since the plasma is nontransparent for the wave in the studied frequency range. The radial distributions of these fields look very similar. However, they are easily distinguishable in the performed calculations due to a significant difference in the radial phase change within the dielectric rod and the layer for these modes, $\Delta\Phi = k_{d1}R_1 + k_{d2}(R_3 - R_2)$. The phase change is $\Delta\Phi = 0.254$ for the mode with the lowest frequency, and $\Delta\Phi = 2.576$ for the mode with the highest frequency.

The azimuthal electric field of the mode that corresponds to the middle frequency $\omega = 1.142|\omega_e|$ reaches its maximum at the interface $r = R_1$ and does not change its sign within the waveguide.

IV. CONCLUSIONS

The dispersion properties of azimuthal surface waves (ASWs) along with their excitation by annular beams of charged particles were studied in detail for the case of the cylindrical waveguide structure: central plasma column–coaxial dielectric layer–outer metal waveguide wall.[10] Two modes of ASWs, ordinary ASWs with the components E_z, B_r, B_φ, and extraordinary ASWs with the components B_z, E_r, E_φ, were demonstrated to propagate independently in such structures. Zeroth radial modes of OASWs were shown to be suppressed in such waveguides.

However, the present introduction of an internal dielectric rod (e.g., as helix support in a plasma TWT) causes the appearance of an additional interface dielectric plasma, which in turn gives rise to the existence of one more solution of the dispersion relation for the studied surface-type waves. This can be of practical interest for designing plasma electronic devices for wideband communication systems.

Introduction of the cylindrical metallic helix sheath results in coupling of OASWs and XASWs. In this case, the zeroth radial modes of OASWs play the role of driven waves. The coupling causes the appearance of one solution more of the dispersion relation of ASWs with positive azimuthal wavenumbers. XASWs are known to be effectively excited by annular electron beams gyrating in the external axial static magnetic field around the plasma column (see, e.g., Refs. 27–29) This is possible due to the presence of the azimuthal electric wave field E_φ of the superposition of XASWs, which is parallel to the annular beam velocity. The presence of the axial electric wave field E_z in the superposition of ASWs coupled by the helix sheath makes it possible to excite ASWs by an axial annular electron beam, being an element of traveling wave tubes (TWTs). Since ASWs do not transfer their energy in the axial direction, their excitation should be considered as an undesired parasitic phenomenon in such coaxial TWTs, where the helix is supported by the inner dielectric rod. Therefore, the analysis provided in this paper can be useful to avoid parasitic energy losses. The helix sheath uses to play the role of the slow-wave structure in TWTs. The decrease in the helix pitch angle is shown to result in an increase in the eigenfrequency of the undesired ASWs.

Thus, the present detailed analysis of ASW dispersion properties in dependence on the waveguide parameters: geometrical dimensions, plasma particle density, external axial static magnetic field, magnitude and sign of azimuthal wavenumber, pitch angle of the metallic helix, and dielectric constants, can be of interest for the suppression of parasitic waves in plasma-loaded coaxial TWTs, operating in the gigahertz range of frequencies.

ACKNOWLEDGMENTS

This work was partially supported by the Ministry of Education and Science of Ukraine Research Grant No. 0119U002526.

APPENDIX: COMPONENTS OF THE DISPERSION RELATION

In Eq. (14), the matrix elements are as follows:

$$a_{11} = J_m(x_1),\ a_{13} = -I_m(x_3),\ a_{14} = -K_m(x_3),\quad a_{12} = a_{15} = a_{16} = a_{17} = a_{18} = 0, \tag{A1}$$

$$a_{22} = J_m(x_1),\ a_{25} = -I_m(x_2),\ a_{26} = -K_m(x_2),\quad a_{21} = a_{23} = a_{24} = a_{27} = a_{28} = 0, \tag{A2}$$

$$a_{32} = x_1 J'_m(x_1),\ a_{35} = -x_2 I'_m(x_2),\ a_{36} = -x_2 K'_m(x_2),\quad a_{31} = a_{33} = a_{34} = a_{37} = a_{38} = 0, \tag{A3}$$

$$a_{41} = x_1^{-1} J'_m(x_1),\ a_{43} = x_3^{-1} I'_m(x_3) + m\mu x_3^{-2} I_m(x_3),\quad a_{44} = x_3^{-1} K'_m(x_3) + m\mu x_3^{-2} K_m(x_3),\quad a_{42} = a_{45} = a_{46} = a_{47} = a_{48} = 0, \tag{A4}$$

$$a_{55} = I_m(x_4),\ a_{56} = K_m(x_4),\quad a_{58} = N_m(x_6) J_m(x_7) - J_m(x_6) N_m(x_7),\quad a_{51} = a_{52} = a_{53} = a_{54} = a_{57} = 0, \tag{A5}$$

$$a_{63} = x_5^{-1} I'_m(x_5) + m\mu x_5^{-2} I_m(x_5),\quad a_{64} = x_5^{-1} K'_m(x_5) + m\mu x_5^{-2} K_m(x_5), \tag{A6}$$

$$a_{67} = x_6^{-1}\left[J'_m(x_6) N'_m(x_7) - N'_m(x_6) J'_m(x_7)\right],\quad a_{61} = a_{62} = a_{65} = a_{66} = a_{68} = 0,\quad a_{71} = a_{72} = a_{73} = a_{74} = a_{75} = a_{76} = 0, \tag{A7}$$

$$a_{77} = x_8 x_5^{-1} \cos\theta\left[J'_m(x_6) N'_m(x_7) - N'_m(x_6) J'_m(x_7)\right],\quad a_{78} = \sin\theta\left[J_m(x_6) N_m(x_7) - N_m(x_6) J_m(x_7)\right],\quad a_{81} = a_{82} = 0,\ a_{83} = \sin\theta I_m(x_5),\ a_{84} = \sin\theta K_m(x_5),\quad a_{85} = \cos\theta x_4 x_8^{-1} I'_m(x_4),\quad a_{86} = \cos\theta x_4 x_8^{-1} K'_m(x_4),\quad a_{87} = \sin\theta\left[N_m(x_6) J'_m(x_7) - J_m(x_6) N'_m(x_7)\right],\quad a_{88} = x_6 x_8^{-1} \cos\theta\left[N'_m(x_6) J_m(x_7) - J'_m(x_6) N J_m(x_7)\right]. \tag{A8}$$

The following notations are applied in Eqs. (A1)–(A8):

$$x_1 = k_{d1} R_1,\quad x_2 = k_o R_1,\quad x_3 = k_\perp R_1,\quad x_4 = k_o R_2,\quad x_5 = k_\perp R_2,\quad x_6 = k_{d2} R_2,\quad x_7 = k_{d2} R_3,\quad x_8 = k R_2.$$

DATA AVAILABILITY

The data that support the findings of this study are available within the article.

REFERENCES

[1] D. F. G. Minenna, F. André, Y. Elskens, J.-F. Auboin, F. Doveil, J. Puech, and É. Duverdier, "The traveling-wave tube in the history of telecommunication," Eur. Phys. J. H **44**, 1–36 (2019).

[2] X. Hong-Quan and L. Pu-Kun, "Theoretical analysis of a relativistic travelling wave tube filled with plasma," Chin. Phys. **16**(3), 766–771 (2007).

[3] A. Abdoli-Arani, "Dispersion relation of TM mode electromagnetic waves in the rippled-wall elliptical plasma and dielectric waveguide in presence of elliptical annular electron beam," IEEE Trans. Plasma Sci. **41**(9), 2480–2488 (2013).

[4] S. K. Datta, L. Kumar, and B. Basu, "Pierce-type one-dimensional Eulerian hydrodynamic analysis of a plasma-filled helix traveling-wave tube," IEEE Trans. Electron Devices **58**(3), 882–890 (2011).

[5] Z. Lu, W. Ge, R. Wen, Z. Su, Z. Wang, T. Tang, H. Gong, and Y. Gong, "High power folded waveguide traveling wave tube based on variable-width technology," Phys. Plasmas **26**(5), 053106 (2019).

[6] W. Shao, D. Xu, Z. Wang, H. Gong, Z. Lu, Z. Duan, Y. Wei, Y. Gong, and S. Aditya, "Stacked dual beam electron optical system for THz integrated wideband traveling wave tube," Phys. Plasmas **26**(6), 063106 (2019).

[7] X. Lei, Y. Zhao, S. Fang, Q. Li, G. Wu, P. Yin, X. Jiang, H. Yin, J. Xu, L. Yue, Y. Wei, and W. Liu, "One-dimensional nonlinear analysis of sine waveguide traveling-wave tubes," Phys. Plasmas **26**(9), 092301 (2019).

[8] M. C. de Sousa, F. Doveil, Y. Elskens, and I. L. Caldas, "Wave–particle interactions in a long traveling wave tube with upgraded helix," Phys. Plasmas **27**(9), 093108 (2020).

[9] M. Nejati and L. Rajaei, "The effect of degenerate plasma on the frequency spectra of slow waves in helix traveling-wave tube," IEEE Trans. Plasma Sci. **47**(5), 2571–2581 (2019).

[10] V. Girka, I. Girka, and M. Thumm, *Surface Flute Waves in Plasmas. Theory and Applications* (Springer-Verlag, Cham, Heidelberg, New York, Dordrecht, London, 2014).

[11] G. S. Nusinovich, Y. Carmel, A. G. Shkvarunets, J. C. Rodgers, T. M. Antonsen, V. L. Granatstein, Y. P. Bliokh, D. M. Goebel, and J. P. Verboncoeur, "The Pasotron: Progress in the theory and experiments," IEEE Trans. Electron Devices **52**(5), 845–856 (2005).

[12] T. Anderson, *Plasma Antennas* (Artech House, Boston, London, 2011).

[13] I. Alexeff, T. Anderson, E. Farshi, N. Karnam, and N. R. Pulasani, "Recent results for plasma antennas," Phys. Plasmas **15**(5), 057104 (2008).

[14] V. O. Girka, I. O. Girka, and I. V. Pavlenko, "Electrodynamic model of the gas discharge sustained by azimuthal surface waves," Contrib. Plasma Phys. **41**(4), 393–406 (2001).

[15] T. Ishijima, H. Toyoda, Y. Takanishi, and H. Sugai, "Design of large-area surface wave plasma excited by slotted waveguide antennas with novel power divider," Jpn. J. Appl. Phys., Part 1 **50**(3R), 036002 (2011).

[16] K. Ostrikov, E. C. Neyts, and M. Meyyappan, "Plasma nanoscience: From nano-solids in plasmas to nano-plasmas in solids," Adv. Phys. **62**(2), 113–224 (2013).

[17] C. M. Ferreira and M. Moisan, *Microwave Discharges: Fundamentals and Applications* (Springer Science & Business Media, 2013).

[18] Y. M. Aliev, H. Schlüter, and A. Shivarova, *Guided-Wave-Produced Plasmas* (Springer-Verlag, Berlin, Heidelberg, 2000).

[19] V. A. Girka and I. A. Girka, "Asymmetric long-wavelength surface modes of isotropic plasma waveguides," Plasma Phys. Rep. **28**(8), 682–689 (2002).

[20] V. O. Girka and I. O. Girka, "Asymmetric long-wavelength surface modes in magnetized plasma waveguides entirely filled with plasma," Plasma Phys. Rep. **28**(11), 916–924 (2002).

[21] V. O. Girka, I. O. Girka, I. V. Pavlenko, O. I. Girka, and A. V. Girka, "Coupled azimuthal modes propagating in current-carrying plasma waveguides," J. Plasma Phys. **78**(2), 105–123 (2012).

[22] M. Abramowitz and I. Stegun, *Handbook of Mathematical Functions with Formulas, Graphs, and Mathematical Tables*, Applied Mathematics Series (National Bureau of Standards, Washington, 1972).

[23] A. F. Alexandrov, L. S. Bogdankevich, and A. A. Rukhadze, *Principles of Plasma Electrodynamics* (Springer, Berlin, 1984).

[24]I. O. Girka and P. K. Kovtun, "Azimuthal surface waves in a magnetized plasma," Tech. Phys. **43**(12), 1424–1427 (1998).
[25]V. O. Girka, I. O. Girka, and I. V. Pavlenko, "Excitation of ion azimuthal surface modes in a magnetized plasma by annular flow of light ions," Prog. Electromagn. Res. M **21**, 267–278 (2011).
[26]V. A. Girka, I. A. Girka, A. N. Kondratenko, and V. I. Tkachenko, "Azimuthal surface waves of magnetoactive plasma waveguides," Sov. J. Commun. Technol. Electron. **33**(8), 37–41 (1988).
[27]I. O. Girka and M. Thumm, "Excitation of azimuthal surface modes above the upper-hybrid frequency by external relativistic flows of electrons in coaxial plasma-vacuum waveguide," IEEE Trans. Plasma Sci. **44**(11), 2859–2866 (2016).
[28]O. S. Blednov, V. O. Girka, I. O. Girka, and I. V. Pavlenko, "Excitation of the azimuthal surface waves in electron cyclotron frequency range by rotating electron beam in a coaxial waveguide," IEEE Trans. Plasma Sci. **42**(3), 735–741 (2014).
[29]I. O. Girka, I. V. Pavlenko, and M. Thumm, "Excitation of higher radial modes of azimuthal surface waves in the electron cyclotron frequency range by rotating relativistic flow of electrons in cylindrical wave-guides partially filled by plasmas," Phys. Plasmas **25**(5), 052109 (2018).